

RESEARCH

Open Access



# Balancing adipocyte production and lipid metabolism to treat obesity-induced diabetes with a novel proteoglycan from *Ganoderma lucidum*

YingXin Wang<sup>1</sup>, Fanzhen Yu<sup>1</sup>, Xinru Zheng<sup>1</sup>, Jiaqi Li<sup>1</sup>, Zeng Zhang<sup>2</sup>, Qianqian Zhang<sup>1</sup>, Jieying Chen<sup>1</sup>, Yanming He<sup>2\*</sup>, Hongjie Yang<sup>2\*</sup> and Ping Zhou<sup>1\*</sup>

## Abstract

Obesity is often accompanied by metabolic disorder and insulin resistance, resulting in type 2 diabetes. Based on previous findings, *FYGL*, a natural hyperbranched proteoglycan extracted from the *G. lucidum* fruiting body, can decrease blood glucose and reduce body weight in diabetic mice. In this article, the underlying mechanism of *FYGL* in ameliorating obesity-induced diabetes was further investigated both in vivo and in vitro. *FYGL* upregulated expression of metabolic genes related to fatty acid biosynthesis, fatty acid  $\beta$ -oxidation and thermogenesis; downregulated the expression of insulin resistance-related genes; and significantly increased the number of beige adipocytes in *db/db* mice. In addition, *FYGL* inhibited preadipocyte differentiation of 3T3-L1 cells by increasing the expression of FABP-4. *FYGL* not only promoted fatty acid synthesis but also more significantly promoted triglyceride degradation and metabolism by activating the AMPK signalling pathway, therefore preventing fat accumulation, balancing adipocyte production and lipid metabolism, and regulating metabolic disorders and unhealthy obesity. *FYGL* could be used as a promising pharmacological agent for the treatment of metabolic disorder-related obesity.

**Keywords** Metabolic disorder, Obesity, Diabetes, *Ganoderma lucidum*, Adipocytes, Lipid metabolism, 3T3-L1, AMPK signalling pathway

## Introduction

Type 2 diabetes mellitus (T2DM) is a chronic degenerative disease, and 60% of T2DM patients are obese as a result of metabolic disorder and insulin resistance as well as impaired energy homeostasis [1–6]. Adipose tissues play an important role in surplus energy storage and energy metabolism [4]. Adipose tissue comprises white adipose tissue (WAT), brown adipose tissue and beige adipose tissue. White adipose tissue mainly functions to store fat in the form of lipid droplets and secrete adipokines to regulate the metabolism of tissues such as muscle and liver tissues [7]. Brown and beige adipose tissues mainly act to dissipate excess energy through thermogenesis to maintain a stable body weight, and secrete

\*Correspondence:

Yanming He  
heyanning176@163.com  
Hongjie Yang  
yanghongjie1964@aliyun.com  
Ping Zhou  
pingzhou@fudan.edu.cn

<sup>1</sup> State Key Laboratory of Molecular Engineering of Polymers, Department of Macromolecular Science, Fudan University, Shanghai 200433, China

<sup>2</sup> Yueyang Hospital of Integrated Traditional Chinese and Western Medicine, Shanghai University of Traditional Chinese Medicine, Shanghai 200437, China



© The Author(s) 2023. **Open Access** This article is licensed under a Creative Commons Attribution 4.0 International License, which permits use, sharing, adaptation, distribution and reproduction in any medium or format, as long as you give appropriate credit to the original author(s) and the source, provide a link to the Creative Commons licence, and indicate if changes were made. The images or other third party material in this article are included in the article's Creative Commons licence, unless indicated otherwise in a credit line to the material. If material is not included in the article's Creative Commons licence and your intended use is not permitted by statutory regulation or exceeds the permitted use, you will need to obtain permission directly from the copyright holder. To view a copy of this licence, visit <http://creativecommons.org/licenses/by/4.0/>. The Creative Commons Public Domain Dedication waiver (<http://creativecommons.org/publicdomain/zero/1.0/>) applies to the data made available in this article, unless otherwise stated in a credit line to the data.

many batokines to affect the physiology of a variety of organ systems and tissues, such as liver, heart and muscle [8, 9]. Accumulating evidence has suggested that a high ratio of white to beige adipocytes is associated with insulin resistance [3, 5]. The beige adipose tissue play more roles for controlling the metabolically unhealthy obesity than other adipose tissue [5].

Adipocytes are differentiated from preadipocytes, therefore, many studies have focused on inhibiting the differentiation of preadipocytes to treat obesity in addition to regulating lipid metabolism [10, 11]. Mesenchymal stem cells (MSCs) undergo a two-step process to differentiate into adipocytes: MSCs first differentiate into preadipocytes, and then preadipocytes continue to differentiate into mature adipocytes [12, 13]. During adipogenesis, the peroxisome proliferator-activated receptor gamma (PPAR $\gamma$ ) and CCAAT/enhancer-binding protein  $\alpha$  (C/EBP $\alpha$ ) are marker proteins for preadipocytes differentiating into mature adipocytes [14, 15]. Subsequently, fatty acids are synthesized in conjunction with the expressions of acetyl-CoA carboxylase (ACC $\alpha$ ) and fatty acid synthase (FAS). Moreover, mature adipocytes further synthesize triglycerides, which aggregate to form lipid droplets [16]. In addition, the triglycerides in lipid droplets are degraded in conjunction with the expressions of adipose triglyceride lipase (ATGL), hormone-sensitive lipase (HSL) [17, 18], which are regulated by the AMP-activated protein kinase  $\alpha$  (AMPK  $\alpha$ ) signalling pathway; thermogenesis in beige adipose tissue is also regulated by this pathway [19, 20]. Based on these results, finding an effective agent to regulate metabolic disorders and control obesity-induced diabetes is very important.

Some anti-obesity drugs, such as orlistat and liraglutide, have been applied clinically in recent years [21, 22]. Orlistat controls body weight by inhibiting pancreatic lipases but has side effects, such as faecal incontinence and flatulence [23]. Liraglutide controls body weight by suppressing gastric emptying and food intake, increasing satiety, and limiting nutrient absorption by increasing pancreatic  $\beta$  cell proliferation, regenerating  $\beta$  cells, and alleviating insulin resistance, but also has side effects such as nausea, vomiting, and diarrhoea [24]. Metformin, a first-line therapeutic agent for diabetes, is an AMPK activator capable of increasing insulin sensitivity and decreasing body weight, but it also has side effects such as abdominal distension, diarrhoea and gastrointestinal intolerance [25].

Previously, Teng et al. extracted a proteoglycan called *FYGL* (Fudan-Yueyang *G. lucidum*) from the fruiting body of *Ganoderma lucidum*, a traditional Chinese medicinal herb used for immunoregulation, anti-inflammation, anti-diabetes and anti-cancer [26, 27]. The dominant sequence of *FYGL* is shown in Fig. 1 [28, 29].

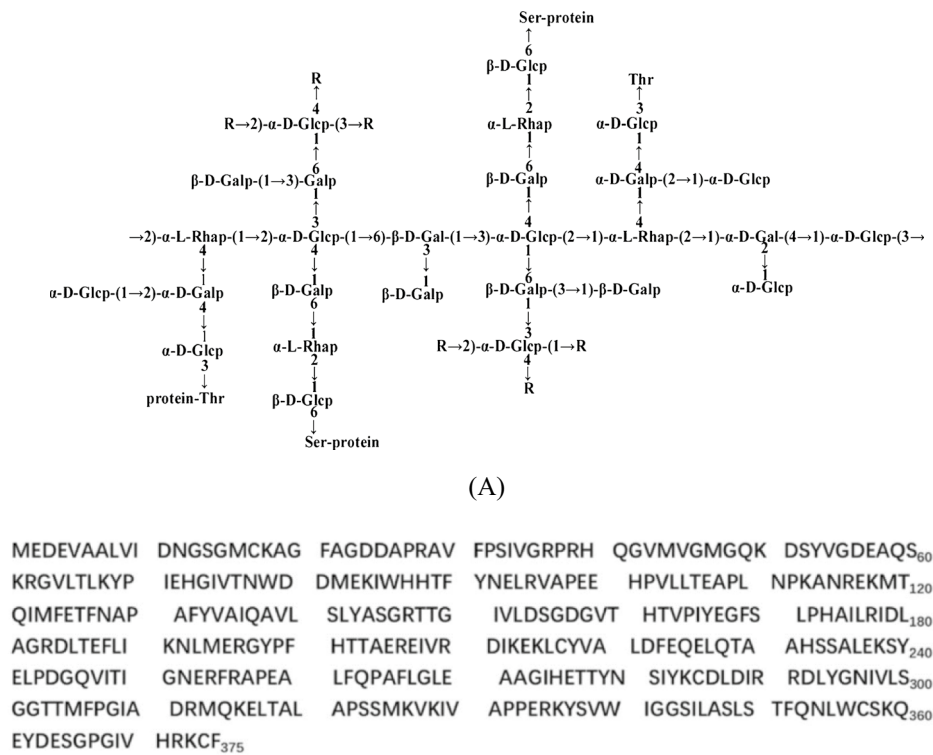
*FYGL* is a hyperbranched proteoglycan with a molecular weight of  $2.6 \times 10^5$  Da and a saccharide: protein ratio of 77:17 [28, 29]. The content of *FYGL* in *Ganoderma lucidum* is about 1% [28]. *FYGL* has been proven capable of decreasing fasting blood glucose through inhibition of the activity of protein tyrosine phosphatase 1 B (PTP1B), an insulin resistance receptor, both in vitro [30] and in vivo [31, 32], as well as reducing body weight in *ob/ob* mice [33]. However, the underlying mechanism by which *FYGL* controls body weight is unknown.

In this work, the mechanism of *FYGL* against obesity-induced diabetes was investigated both in vivo and in vitro. In in vivo studies, *db/db* mice, a specific model of obesity and diabetes resulting from receptor leptin resistance, were used in this work. Because body weight (Fig. 2) and basic metabolic data (including blood glucose, serum insulin level, glycosylated haemoglobin as well as serum triglycerides (TG), total cholesterol (TC), low density lipoprotein-cholesterol (LDL-c), high density lipoprotein-cholesterol (HDL-c) of the animals have been studied and published previously (Figure S1 and S2 in Supplementary materials) [34], this paper focused on the function and mechanism of *FYGL* controlling obesity. The beige adipose tissue from *db/db* diabetic mice was used to analyse the expression of genes related to fatty acid biosynthesis and metabolism, thermogenesis, and insulin sensitivity, which are beneficial for beige adipose tissue functions. In in vitro studies, the 3T3-L1 cell line was used to investigate the underlying mechanism by which *FYGL* alleviates obesity. 3T3-L1 cells are preadipocytes and normally differentiate into mature adipocytes [35]. The effects of *FYGL* on preadipocyte differentiation and mature adipocyte lipid metabolism were investigated in terms of gene and protein expressions in preadipocytes as well as signalling pathways of lipid metabolism in mature adipocytes.

## Materials and methods

### Materials

Fruiting bodies of *G. lucidum* grown in northeast China were purchased from Leiyunshang Pharmaceutical Co. Ltd (Shanghai, China). The preparation of *FYGL* was described in previous work [31]. Dulbecco's modified Eagle's medium (DMEM), foetal bovine serum (FBS), and penicillin/streptomycin antibiotics were purchased from Gibco Co. Ltd (USA). 3T3-L1 cells were obtained from Procell Life Science & Technology Co. Ltd (Wuhan, China). Fluorescein isothiocyanate (FITC), 4',6-diamidino-2-phenylindole (DAPI), rhodamine-labelled phalloidin and super ECL detection reagent were provided by Yeasen Co. Ltd (Shanghai, China). A cell counting kit-8 (CCK-8), a modified oil red O staining kit, a bicinchoninic acid (BCA) kit, newborn calf



(A)

**Fig. 1** **A** The dominant polysaccharide sequence of *FYGL* characterized by chemical analysis and NMR spectroscopy [29]. Rs represents the carbohydrate residues of  $\rightarrow 2,4$ - $\alpha$ -L-Rhap-(1  $\rightarrow$ ,  $\rightarrow 6$ - $\beta$ -D-Galp-1  $\rightarrow$ , Araf(1  $\rightarrow$  or  $\rightarrow 3,6$ )- $\beta$ -D-Galp-(1  $\rightarrow$ ). Protein moieties are covalently bonded with carbohydrate moieties by Ser and Thr residues in the -O- linkage. **B** The dominant sequence of the protein moieties of *FYGL* characterized by mass spectrometry

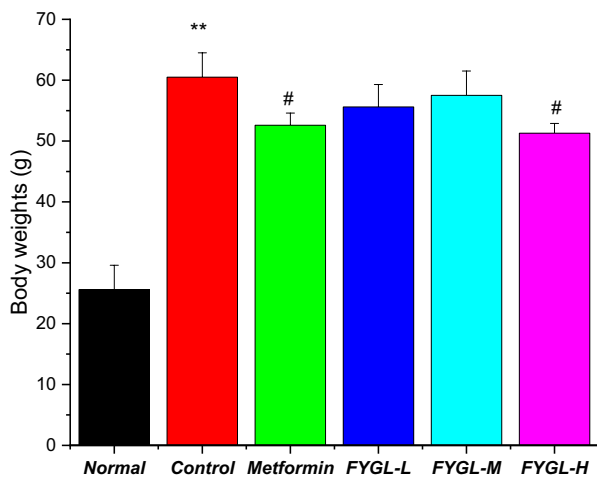


**Fig. 2** Body weights of *db/db* mice treated with *FYGL* for 8 weeks. \* $P < 0.05$ , \*\* $P < 0.01$  vs. control group [34]

peroxidase (HRP)-labelled secondary antibody were purchased from Beyotime Co. Ltd (Shanghai, China). Dimethyl sulfoxide (DMSO) was provided by Sigma-Aldrich (Taufkirchen, Germany). Triglyceride (TG) assay kits were obtained from Jiancheng Bioengineering Institute (Nanjing, China). The RNAprep pure cell kit was acquired from TIANGEN Biotech Co. Ltd (Beijing, China). The HiScript III All-in-one RT SuperMix kit (#R333) and Taq Pro Universal SYBR qPCR Master Mix kit (#Q712) were purchased from Vazyme Biotech Co. Ltd (Nanjing, China). Primary antibodies against peroxisome proliferator-activated receptor gamma (PPAR, A11183), lipoprotein lipase (LPL, A16252), and  $\beta$ -actin (AC026) were purchased from ABclonal Technology Co. Ltd (Wuhan, China). Primary antibodies against CCAAT/enhancer-binding protein  $\alpha$  (C/EBP $\alpha$ , ab40764), fatty acid synthase (FAS, ab128870), fatty acid binding protein 4 (FABP-4, ab92501), adipose triglyceride lipase (ATGL, ab109251), AMPK $\alpha$ 1 (ab32047), AMPK $\alpha$ 1 (phospho T183)+AMPK $\alpha$ 2 (phospho T172) (p-AMPK $\alpha$ , ab133448) were purchased from Abcam (Cambridge, MA, USA). Primary antibodies against

serum (NCS), RIPA lysis buffer, dexamethasone, 3-isobutyl-1-methylxanthine (IBMX), paraformaldehyde, Triton X-100, anti-rabbit IgG (H+L), and a horseradish

hormone-sensitive lipase (HSL, #4107) were purchased from Cell Signaling Technology (CST, Beverly, MA, USA).

#### Animal trial

All male C57BLKS/J-Diabetes Genes (BKS-DB) mice (4 weeks old) and wild-type BKS-DB (*db/m*) mice were purchased from GemPharmatech Co. Ltd, Nanjing, China. Mice were housed in the specific pathogen-free (SPF) animal experimental center of the school of pharmacy, Fudan University, at a constant temperature ( $22 \pm 2$  °C) on a 12 h/12 h light/dark cycle and were provided standard food and water. All animal trials were conducted following protocols approved by the Fudan University Institutional Animal Care and Use Committee. Subsequent experimental procedures were performed according to the method described in previous works [36, 37]. After adaptation for 4 weeks, the mice were divided into six groups (12 mice/group): (1) *db/m* mice + saline (normal); (2) *db/db* + saline (control); (3) *db/db* + metformin (225 mg/kg/d, positive); (4–6) *db/db* + *FYGL* (225 mg/kg/d, 450 mg/kg/d, 900 mg/kg/d, as low (*FYGL-L*), middle (*FYGL-M*), high (*FYGL-H*) dose, respectively). Six groups were orally administrated with saline or the corresponding concentrations of drugs for 8 weeks. During the experiment, the body weight of all the mice was recorded weekly as a basis for gavage dose, and FBG levels of blood samples from the tail vein were examined weekly [34]. After 7 weeks of drug treatment, all the mice were sacrificed by cervical dislocation.

#### Histopathological analysis of beige adipose tissue

Beige adipose tissue was extracted from the scapulae of *db/db* mice and were fixed, sectioned, and mounted. The sections were stained with haematoxylin and eosin (H&E) and observed by microscopy (NanoZoomer 2.0-HT, Japan). Adipocyte numbers are shown as ratios of the adipocyte number to the area of the selected region (a randomly selected circle with an area of 0.1 mm<sup>2</sup>) in the images.

#### RNA sequencing (RNA-seq) analysis of beige adipose tissue

Total RNA was extracted from beige adipose tissue. RNA purity was checked using a NanoPhotometer<sup>®</sup> spectrophotometer (IMPLEN, CA, USA). RNA integrity was assessed using the RNA Nano 6000 Assay Kit for the Bioanalyzer 2100 system (Agilent Technologies, CA, USA). Sequencing libraries were generated using the NEBNext<sup>®</sup> UltraTM RNA Library Prep Kit for Illumina<sup>®</sup> (NEB, USA) following the manufacturer's recommendations, and index codes were added to attribute sequences to each sample. Clustering of the index-coded samples was performed on a cBot Cluster Generation System using

TruSeq PE Cluster Kit v3-cBot-HS (Illumina) according to the manufacturer's instructions. After cluster generation, the library preparations were sequenced on the Illumina NovaSeq platform, and 150 bp paired-end reads were generated. Every group was analysed with three biological replicates. Differential expression analyses between two conditions or groups (two biological replicates per condition) were performed using the DESeq2 R package (1.16.1). Genes with an adjusted *P* value of < 0.05 determined by DESeq2 were considered differentially expressed. Gene Ontology (GO) enrichment analysis of the differentially expressed genes was implemented in the clusterProfiler R package, in which gene length bias was corrected. GO terms with a corrected *P* value of less than 0.05 were considered significantly enriched with differentially expressed genes. The clusterProfiler R package was used to test the statistical enrichment of the differentially expressed genes in Kyoto Encyclopedia of Genes and Genomes (KEGG) for signalling pathway analysis.

#### Cell culture and treatment

3T3-L1 preadipocytes were maintained in DMEM supplemented with 10% NCS and 1% penicillin–streptomycin (basal medium I, BMI). When the cells were confluent (Day 0), adipocyte differentiation was induced by treatment with a cocktail of 5 µg/mL insulin, 1 µM dexamethasone, and 0.5 mM isobutyl methylxanthine in DMEM supplemented with 10% FBS and 1% penicillin–streptomycin (differentiation medium I, DMI). After 48 h (Day 2), the medium was changed to DMEM containing 10% FBS, 1% penicillin–streptomycin, and 5 µg/mL insulin for 48 h (differentiation medium II, DMII). On Day 4, insulin was removed from the medium, and the cells were maintained in DMEM supplemented with 10% FBS and 1% penicillin–streptomycin (basal medium II, BMII), and the medium was changed every two days thereafter [38]. During differentiation, cells were treated with different concentrations of *FYGL* (0, 50, 100, 200, 400, and 800 µg/mL). Undifferentiated cells cultured in BMI were used as the blank control group, and differentiated cells cultured in BMI without *FYGL* were used as the model groups.

#### Uptake of *FYGL* in 3T3-L1 cells

Three milligrams of FITC fluorescence agent was dissolved in 0.3 mL of DMSO to prepare a FITC solution with a concentration of 10 mg/mL, and then the solution was diluted to 1 mg/mL with sodium buffer (SB). *FYGL* (10 mg) was dissolved in 10 mL SB to form a 1 mg/mL *FYGL* solution, which was mixed with the diluted FITC solution at a volume ratio of 10: 1. The mixture was stirred at low temperature (ice bath) to allow the formation of fluorescent FITC–*FYGL* complexes. After the

coupling reaction proceeded overnight, the solution was dialyzed with a 1 kDa dialysis bag to filter free FITC and then cryodesiccated.

3T3-L1 cells were seeded on microscope cover glasses in a 24-well plate with a density of  $1 \times 10^4$  cells per well and were incubated with FITC-FYGL complex (200  $\mu\text{g}/\text{mL}$ ) for 4 h. Nuclei and F-actin (filamentous actin) in 3T3-L1 cells were stained by DAPI and phalloidin-TRITC (phalloidin-tetramethyl rhodamine), respectively. Cell images were acquired with a C2<sup>+</sup> laser scanning confocal microscope (Nikon, Japan). Moreover, 3T3-L1 cells were treated with the indicated concentrations of FITC-FYGL (0, 50, 100, 200, 400, 800  $\mu\text{g}/\text{mL}$ ) for 4 h, and then the fluorescence intensity was determined by flow cytometry (Gallios, Beckman Coulter) to visualize the uptake of FYGL in the cells.

#### Measurement of cell viability

Cell viability was measured by a cell counting kit-8 (CCK-8) assay. In brief, 3T3-L1 cells were plated into 96-well plates with a density of  $5 \times 10^3$  cells per well and incubated to near confluence. Some cells were incubated in DMI with different concentrations of FYGL (0, 100, 200, 400, and 800  $\mu\text{g}/\text{mL}$ ) for 24 h. After treatment for 24 h, the medium was discarded, and fresh DMI containing CCK-8 solution was added to the 96-well plates. Approximately 1 h later, a multimode microplate reader (Cytation3, BioTek, U.S.A.) was used to measure the optical density (OD) at 450 nm.

#### Triglyceride quantification

Triglyceride (TG) concentrations were determined using a commercial kit (Jiancheng Bioengineering Institute, China). Briefly, differentiated 3T3-L1 cells were washed twice with phosphate-buffered saline (PBS) and harvested by scraping from the culture plate in PBS containing 1% Triton X-100 on Day 6. Cell homogenates were obtained by sonication, and TG concentrations were determined using a commercial kit according to the manufacturer's instructions. Protein concentrations were measured using the bicinchoninic acid (BCA) protein assay kit (Beyotime, China) and used for quantification of proteins in samples.

#### Oil red O staining and quantification

Lipid accumulation in cells was measured by oil red O staining. Differentiated 3T3-L1 cells were subjected to oil red O staining with modified oil red O staining kits (Beyotime, China). Briefly, the cells were washed with phosphate-buffered saline (PBS, pH 7.4) and then fixed with 10% (v/v) paraformaldehyde at room temperature for 10 min. Then, the fixation solution was removed, and the cells were washed twice with PBS. The cells were

immersed in washing solution for 20 secs. After the washing solution was discarded, modified oil red O was added and incubated with the cells at room temperature for 20 min. Then, the staining solution was removed, and the cells were washed with washing solution once and PBS twice. Finally, cells stained with oil red O were examined via a polarizing microscope (DM2500P, Leica, Germany). In addition to this gross evaluation, the dye was dissolved in 60% isopropanol solution, and the absorbance was measured at 510 nm for quantification of lipid accumulation.

#### RNA extraction and RT-qPCR analysis

Total RNA was isolated from differentiated 3T3-L1 cells using RNeasy pure cell kits (TIANGEN, China) according to the manufacturer's instructions. Conversion of total RNA to single-stranded cDNA was performed using HiScript III All-in-one RT SuperMix Kits (Vazyme, China). The series of primers of  $\beta$ -actin (as an internal reference), C/EBP $\alpha$ , FABP4, ATGL, and LPL shown in Table 1 were synthesized by Sangon Co. The primers were mixed with cDNA templates, and qPCR was then performed with a Taq Pro Universal SYBR qPCR Master Mix kit (Vazyme, China) on a qPCR instrument (Bio-Rad, Germany) to amplify the DNA of C/EBP $\alpha$ , FABP4, ATGL, and LPL. The melt curves of the cDNA were analysed to determine the specificity of amplification, and quantification of relative mRNA levels was performed using the  $2^{-\Delta\Delta\text{Ct}}$  method with normalization to  $\beta$ -actin mRNA.

#### Protein extraction and immunoblot analysis

Immunoblot analysis was performed according to the method described in a previous report with a minor modification [39]. Differentiated 3T3-L1 cells were lysed in RIPA lysis buffer and centrifuged (12,000 $\times g$ , 10 min, 4°C). Proteins in the lysates were separated by 10% SDS-PAGE and transferred to polyvinylidene fluoride membranes. Then, the membranes were blocked in TBST/5% nonfat dry milk powder; incubated overnight at 4 °C with antibodies against FABP4, PPAR $\gamma$ , CEBP $\alpha$ , AMPK $\alpha$ , p-AMPK $\alpha$ , ATGL, HSL, LPL, and  $\beta$ -actin; and incubated

**Table 1** The primer sequences

Gene	Forward primer (5' to 3')	Reverse primer (5' to 3')
$\beta$ -actin	GGGAATGGGTCAGAAGGACTC	GGTGTGGTGCCAGATCTTCTC
C/EBP $\alpha$	GAAGGTGCTGGAGTTGACCAG	CCTTGACCAAGGAGCTCTCAG
FABP-4	AAGGTGAAGAGCATCATA ACCT	TCACGCCCTTTCATAACACATTCC
ATGL	ATGTTCCCGAGGGAGACCAA	GAGGCTCCGTAGATGTGAGTG
LPL	TTGCCCTAAGGACCCCTGAA	TTGAAGTGGCAGTTAGACACAG

with a goat anti-rabbit secondary antibody at room temperature for 1 h. Finally, enhanced chemiluminescence solution (ECL) was used to detect the proteins on the membranes. The luminescence signals were recorded with a Chemscope3300 mini (Clinx Science Instruments, China). Data were collected from three independent experiments.

### Statistical analysis

All data were analysed by SPSS 20.0 (SPSS, Inc., U.S.), and expressed as the mean  $\pm$  S.D. values. All the data were significantly drawn from a normally distributed population at the 0.05 level, justified by Shapiro–Wilk normality test. One-way ANOVA followed by the Bonferroni correction was performed to analyse the statistical significance of differences among the groups. A value of  $P < 0.05$  was considered statistically significant.

## Results

### Effect of *FYGL* on histopathology of beige adipose tissue in vivo

In the present work, beige adipose tissue in *db/db* mice was subjected to histopathological analysis. Figure 3A shows that the size of beige adipocytes was larger, and the numbers were lower in the control group than in the normal group, whereas treatment with metformin and *FYGL* reduced the size of adipocytes. Semiquantitative analysis of H&E staining in Fig. 3B showed that *FYGL* significantly increased the number of adipocytes per unit area of beige adipose tissue in a dose-dependent manner.

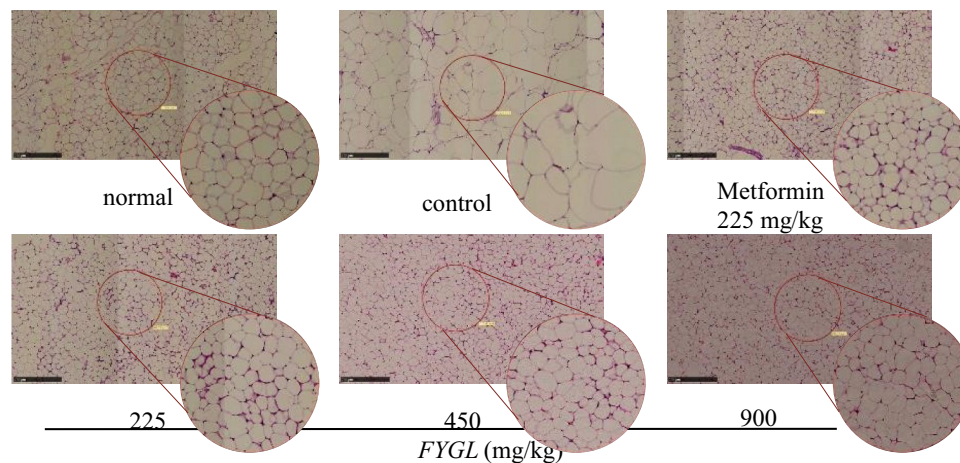
### Effect of *FYGL* on lipid metabolism in vivo

Type 2 diabetes is strongly associated with genes of lipid metabolism [40]. In this work, beige adipose tissue transcriptome sequencing was performed to explore the potential molecular mechanism of lipid metabolism in vivo. As shown in Fig. 4A, the screening results of the differentially expressed genes (DEGs) showed that the ratio of upregulated: downregulated: all differentially expressed genes was approximately 0.5: 0.5: 1 in the metformin and *FYGL* groups compared with the control group, nearly the same as the ratio in the normal group compared to the control group. Figure 4B shows the hierarchical clustering heatmap. The large coloured square patterns represent the upregulated or downregulated genes in the different groups. The change in colour from blue to red indicates a change in the gene expression from downregulation to upregulation. The narrow columns on the left show the pathway-related genes. Figure 4B shows that the colour patterns of the DEGs in the control group were different from those in the normal group for most genes except *Ppp1r3b*, while the colour patterns in the *FYGL* group were similar to those in the

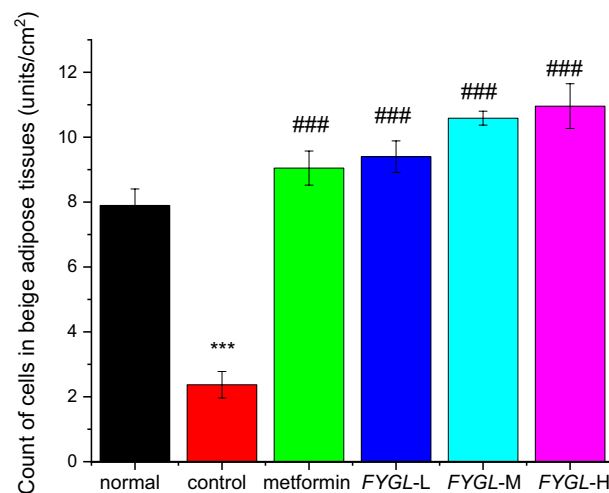
normal group. From the pathway indication in the upper-left corner in Fig. 4B, it can be seen that the DEGs were involved in the pathways of fatty acid synthesis (black), fatty acid oxidation (green), insulin resistance (yellow), and thermogenesis (purple).

As shown in Fig. 4B, *FYGL* increased the mRNA levels of *Ppp1r3b*, *Fasn*, *Acaca*, *CPT2*, and *Acadl* in the beige adipose tissue of *db/db* mice compared to those in the control group. The *Ppp1r3b* gene encodes protein phosphatase 1, which is a critical protein in glycogen metabolism regulated by insulin [41]. The *Fasn* (encoding FAS [42]) and *Acaca* (encoding ACC $\alpha$  [43]) genes are involved in fatty acid synthesis [42, 43]. *CPT2* (encoding CPT-II, carnitine palmitoyl transferase II [44]) and *Acadl* (encoding ACADL, acyl-CoA dehydrogenase long chain [45]) are involved in the  $\beta$ -oxidation of long-chain fatty acids in mitochondria [44, 45]. The imbalance between fatty acid synthesis and degradation can lead to dyslipidaemia, diabetes and cardiovascular disease [46, 47]. Transcript analysis of those genes in beige adipose indicated that *FYGL* could upregulate fatty acid metabolism in vivo. Additionally, as shown in Fig. 4B, *FYGL* upregulated fatty acid degradation genes (*CPT2* and *Acadl*) more significantly than fatty acid synthesis genes (*Fasn* and *Acaca*). In addition, as shown in Fig. 4B, *FYGL* increased the levels of *Cd81* (encoding CD81 [48]) and *Slc25a4* (encoding SLC25A4 [49]) compared to those in the control group, and the levels of these mRNAs in the *FYGL* group were even higher than those in the metformin group. CD81 is a marker of beige adipocyte progenitors. The absence of CD81 leads to diet-induced obesity, insulin resistance, and adipose tissue inflammation [48]. SLC25A4, a mitochondrial ATP/ADP transporter, regulates thermogenesis of beige adipose through UCP1-independent mechanisms [50]. Beige adipocytes can produce heat by metabolizing fatty acids. Transcriptome analysis indicated that *FYGL* could increase the expression of thermogenesis genes (*Cd81* and *Slc25a4*) in beige adipose, as indicated by the transition from blue to red in Fig. 4B. Furthermore, *FYGL* and metformin increased the mRNA levels of *Akt2* (encoding AKT2 [51]) and *Slc2a4* (encoding GLUT-4, glucose transporter-4 [52]), as shown in Fig. 3B. Deficiency of AKT2 and GLUT-4 leads to type 2 diabetes and insulin resistance [51, 53]. The relative study and results have been reported by Pan et al. (see Figure S1 and S2 in Supplementary materials) [34, 54].

The GO (Gene Ontology) database is a comprehensive database describing gene functions, which includes the biological process (BP), cellular component (CC), and molecular function (MF) in ontological categories. Figure 5A shows the bubble plot of the biological processes in the Gene Ontology (GO) enrichment analysis (*FYGL* vs. control), where the redder the dot is, the more



(A)



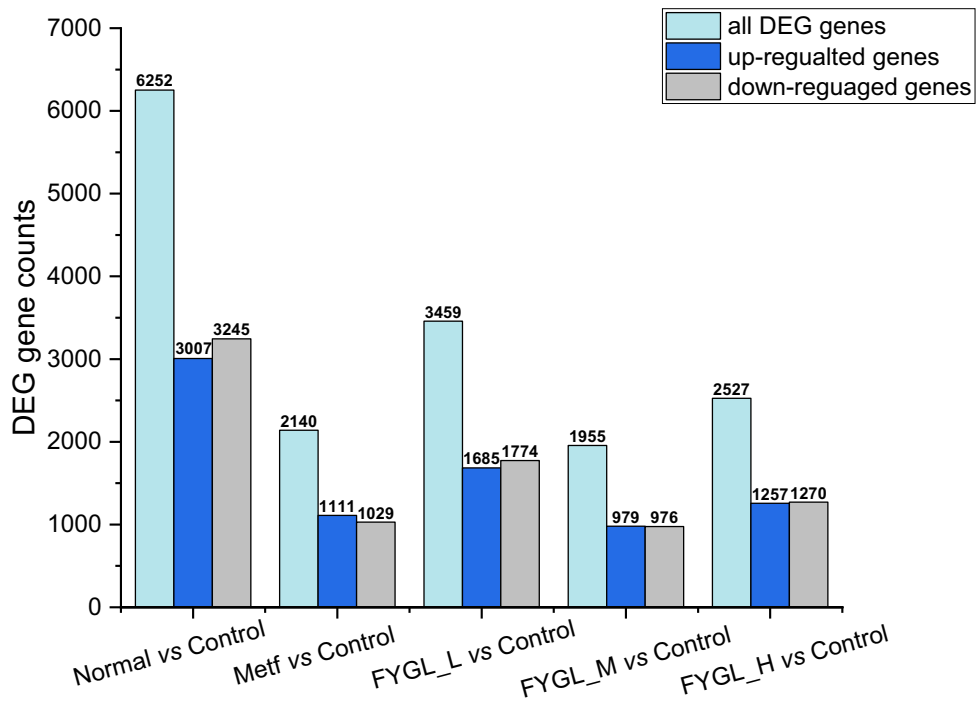
(B)

**Fig. 3** Histopathological analysis of adipocytes in beige adipose tissues. **A** Representative images of H&E-stained beige adipose tissues, magnification 100 $\times$ . The scale bar represents 250  $\mu$ m. **B** Semiquantitative analysis of the adipocyte number per area in beige adipose tissue by Image-Pro Plus 6.0 software. The mean  $\pm$  S.D. values are presented ( $n=6$ ; \*\*\* $P<0.001$  vs. normal; \* $P<0.05$ , \*\* $P<0.01$ , \*\*\* $P<0.001$  vs. control)

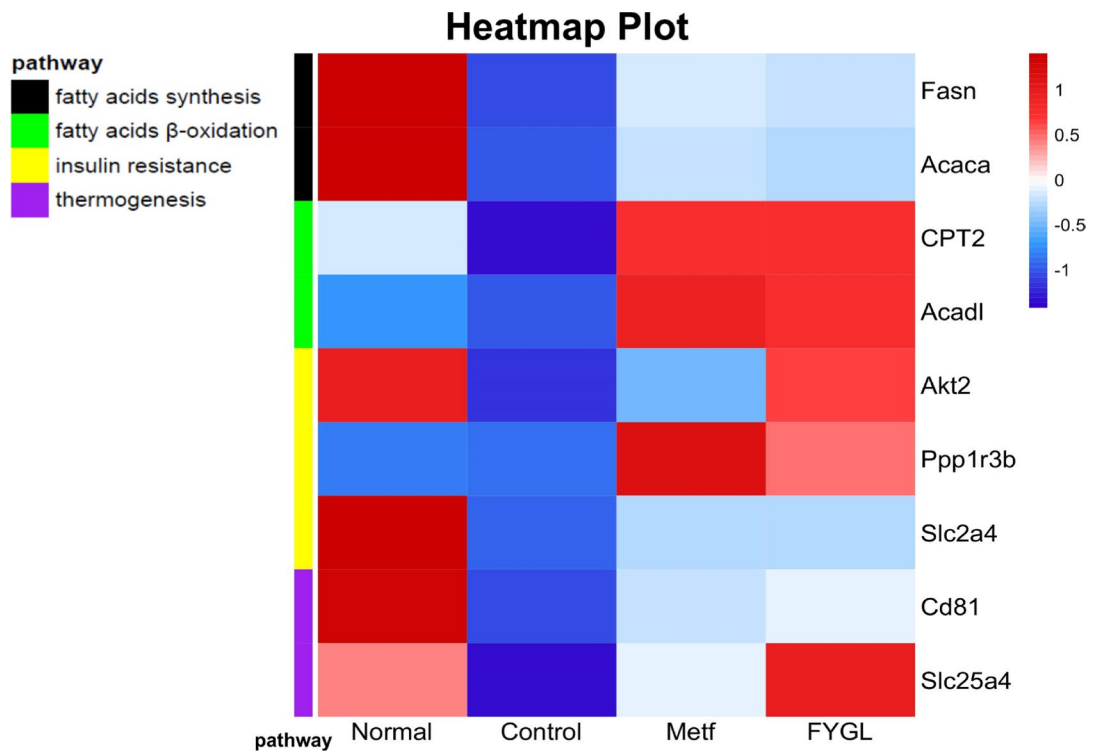
significant the enrichment of the biological process. Figure 5A shows that DEGs were mainly enriched in terms related to the biological processes of cellular respiration, fatty acid metabolism (gene *Fasn* and *Acaca*), tricarboxylic acid metabolism, fatty acid oxidation (gene *CPT2* and *Acadl*), etc., and that *FYGL* restored beige adipose functions in *db/db* mice through those biological processes. Figure 5B is a directed acyclic graph (DAG, *FYGL* vs. control) of the GO biological process enrichment analysis, which indicates the relationship of functions from up- to down- biological processes. Figure 5B shows that

the biological processes were eventually refined to fatty acid metabolism and cellular respiration.

Figure 5C shows the bubble plot of the signalling pathways in the Kyoto Encyclopedia of Genes and Genomes (KEGG) enrichment analysis (*FYGL* vs. control), where the redder the dot is, the more significant the enrichment of the signalling pathway. Figure 5C shows that DEGs were predominantly enriched in signalling pathways related to oxidative phosphorylation, thermogenesis, citrate cycle (TCA cycle), fatty acid metabolism, and fatty acid biosynthesis. The data in Fig. 5C suggest that *FYGL*



(A)



(B)

**Fig. 4** Transcriptome analysis of RNA sequencing of beige adipose tissue in the normal, metformin, and *FYGL* groups compared to the control group. **A** DEG counts. **B** Hierarchical clustering heatmap of the expression profile of the DEGs



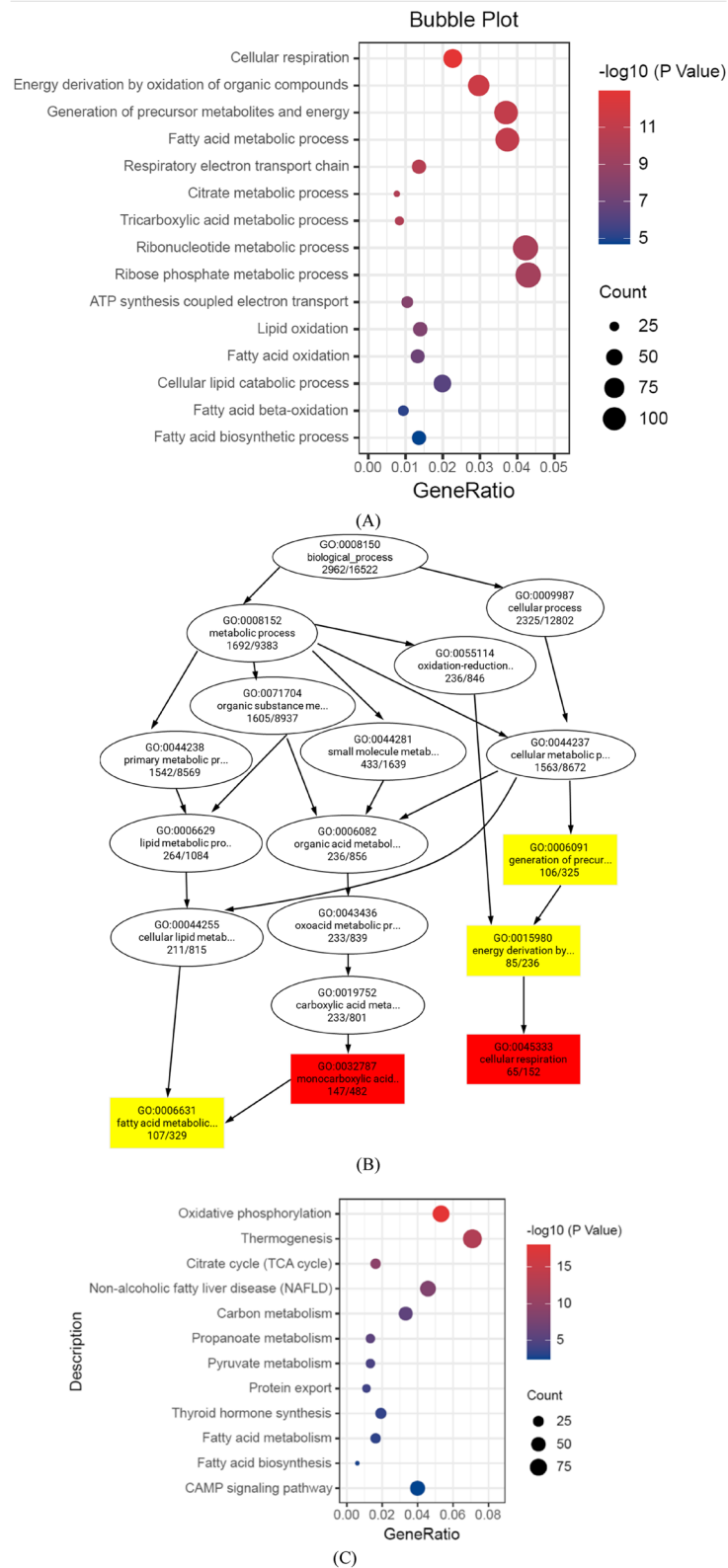


**Fig. 5** GO and KEGG functional enrichment analyses based on the DEGs. **A** Bubble plot of biological processes in the GO enrichment analysis. **B** The directed acyclic graph of biological process in the GO enrichment analysis. **C** Bubble plot of pathways in the KEGG enrichment analysis

promotes the functions of beige adipose through those signalling pathways.

#### Cellular uptake of *FYGL*

To reveal the underlying mechanisms of *FYGL* in mediating biological functions, investigations at the cellular level are necessary. Figure 6A shows the uptake of *FYGL* (200 µg/mL and 400 µg/mL) in 3T3-L1 cells, as measured by confocal laser scanning microscopy, where green fluorescence was found in the cells cultured with FITC-labelled-*FYGL*, indicating that *FYGL* could be taken up well into 3T3-L1 cells. Moreover, the results of flow cytometric analysis of *FYGL* uptake in 3T3-L1 cells are shown in Fig. 6B and C; the peak of the curve shifted to the right as the FITC-*FYGL* concentration increased, and the uptake of *FYGL* in cells occurred in a dose-dependent manner.

#### Effect of *FYGL* on cell viability

To examine the cytotoxicity of *FYGL* in 3T3-L1 adipocytes, cell viability was measured using the CCK-8 assay. Adipocytes were treated with various concentrations of *FYGL* (0–800 µg/mL). The CCK-8 assay results shown in Fig. 6D demonstrate that *FYGL* had no obvious cytotoxicity at concentrations up to 800 µg/mL.

#### Effect of *FYGL* on the accumulation of intracellular triglycerides and lipids

Lipid accumulation in adipocytes is a hallmark of adipogenesis. Excessive accumulation of lipid droplets in adipocytes leads to obesity and insulin resistance [16]. Mature differentiated cells accumulate triglycerides, which then converge to form lipid droplets (LDs). Figure 7A shows that *FYGL* significantly decreased the triglyceride content. Moreover, cell differentiation and lipid accumulation can be identified by oil red O staining and triglyceride assays. Figure 7B shows that the number of lipid droplets (red staining) was markedly increased in cells cultured in differentiation medium (DM) but was significantly decreased when the cells were cultured with *FYGL* (200–400 µg/mL), and Fig. 7C quantitatively shows the effect of *FYGL* on lipid droplet accumulation. *FYGL* inhibited triglyceride accumulation and lipid droplet aggregation in differentiated adipocytes. The mechanism of inhibition was further investigated as follows.

#### Effect of *FYGL* on the expression of adipogenic and lipolytic genes and proteins

Several reports have shown that peroxisome proliferator-activated receptor  $\gamma$  (PPAR $\gamma$ ) and CCAAT/enhancer-binding protein  $\alpha$  (C/EBP $\alpha$ ) are marker proteins of adipocyte differentiation and adipogenesis [12, 55, 56]. To reveal the mechanisms by which *FYGL* inhibits the

accumulation of intracellular triglycerides and lipids, the effect of *FYGL* on the expression of adipogenic and lipolytic genes and proteins was investigated. Figure 8A shows that *FYGL* significantly increased the transcript level of FABP-4 in 3T3-L1 preadipocytes and considerably increased the transcript level of C/EBP $\alpha$  in adipocytes cultured in differentiation medium (Fig. 8B). Moreover, *FYGL* increased the mRNA level of lipolytic genes, such as ATGL (Fig. 8C) and LPL (Fig. 8D).

Furthermore, Western blotting was used to analyse the protein expression of FABP-4, PPAR $\gamma$ , and C/EBP $\alpha$ , as shown in Fig. 9A. *FYGL* greatly increased FABP-4 expression, as shown in Fig. 9B, and markedly decreased PPAR $\gamma$  and C/EBP $\alpha$  expression, as shown in Fig. 9C and D.

#### Effect of *FYGL* on lipid metabolism and the AMPK $\alpha$ signalling pathway

The fatty acid synthase (FAS) and AMPK $\alpha$  signalling pathway play important roles in lipogenic pathways [57]. Activating the AMPK signalling pathway can increase the activity of the lipases of ATGL and HSL, thus promoting the utilization of lipid storage [19, 58–60]. As shown in Fig. 10A and B, *FYGL* increased the protein expression of FAS. Additionally, *FYGL* increased the phosphorylation of AMPK $\alpha$  (Fig. 10C & D) and consequently increased the protein expression of lipolysis markers, such as ATGL (Fig. 10E), HSL (Fig. 10F), and LPL (Fig. 10G).

In addition, *FYGL* increased the protein levels of ATGL (Fig. 10E) and HSL (Fig. 10F) by twofold compared with that of FAS (Fig. 10B) and by 1.5-fold compared with those in the control group at concentrations higher than 200 µg/mL. Therefore, *FYGL* upregulated lipolysis more significantly than fatty acid biosynthesis, consistent with the results in vivo.

#### Discussion

Cypess et al. proved that the amount and activity of beige adipose tissue are inversely correlated with body mass index [61]; the smaller the size and the greater the number of beige adipocytes, the healthier the body [62–64]. Ouellet et al. demonstrated that the activity of beige adipocytes is positively correlated with the level of glucose uptake in cells, which modulates the blood glucose content [65]. Therefore, increasing the number or activation of beige adipocytes could be a potential approach to treat type 2 obesity-induced diabetes [66]. Consistent with those studies, the results of this study showed that beige adipocytes were significantly enlarged in size and decreased in number in *db/db* mice, while these changes were significantly reversed after *FYGL* treatment.

Based on GO database of gene functions and KEGG enrichment analysis of signalling pathways, the results indicated that *FYGL* upregulated the fatty acid

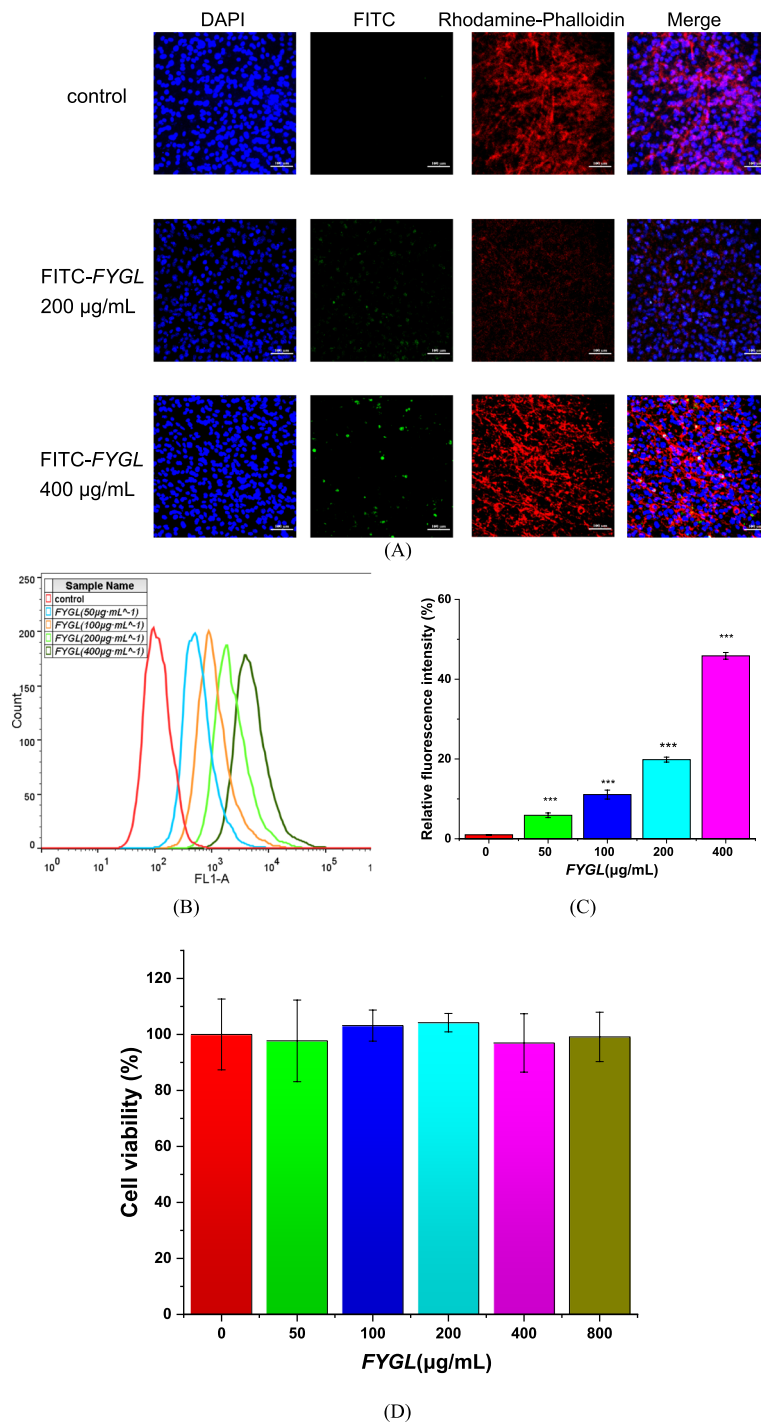


**Fig. 6** **A** Laser confocal scanning microscopy images of FYGL in 3T3-L1 cells at 200× magnification. 3T3-L1 cells were incubated with FITC-FYGL (200 µg/mL) for 4 h; blue (DAPI labelled), red (rhodamine labelled) and green (FITC labelled) represent the nucleus, cytoskeleton and FYGL, respectively. The scale bar represents 100 µm. **B** Flow cytometric analysis of fluorescence. **C** Geometric means calculated by FlowJo software. The data are presented as the mean ± S.D. values ( $n=3$ ). \*\*\* $P<0.001$  vs. control group. **D** Effect of FYGL on cell viability. 3T3-L1 cells were incubated with various concentrations of FYGL (0, 50, 100, 200, 400 and 800 µg·mL<sup>-1</sup>) for 24 h, and cell viability was determined by a CCK-8 assay. The mean ± S.D. values are presented ( $n=6$ )

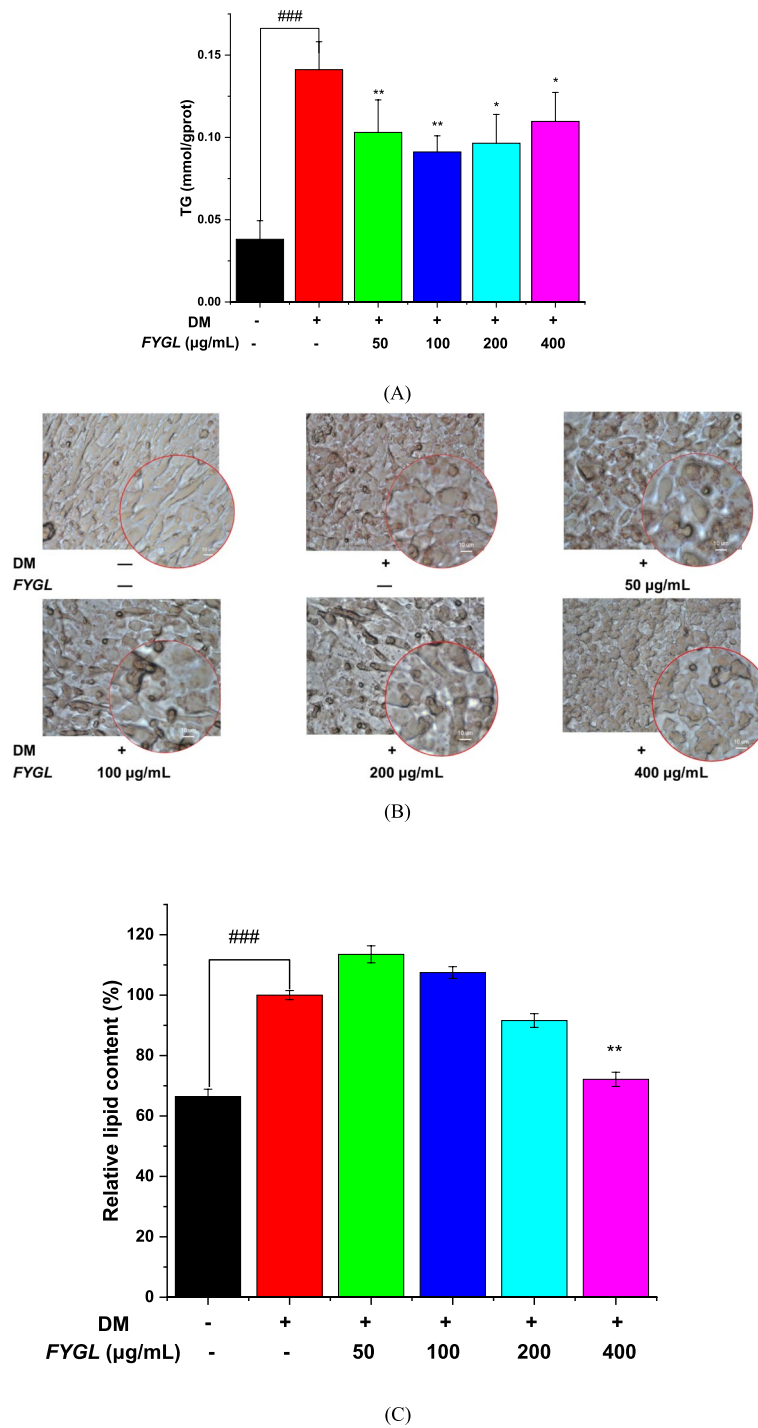


**Fig. 7** Effect of *FYGL* on the inhibition of lipid accumulation in mature adipocytes. Differentiated 3T3-L1 cells were incubated with *FYGL* at concentrations ranging from 0–400 μg/mL. **A** Intracellular TG in mature adipocytes. **B** Intracellular lipid droplets stained by oil red O and visualized by polarized phase contrast microscopy (500×). **C** Intracellular lipid accumulation was quantitatively measured using a microplate reader at an absorbance of 490 nm. Mean ± S.D. values are presented (n=6). ###P<0.001 vs. blank control group, \*\*P<0.01, \*P<0.05 vs. model group

metabolism process and promoted thermogenesis in beige adipocytes. In addition, *FYGL* could balance fatty acid biosynthesis and metabolism to effectively dissipate

energy, therefore reducing insulin resistance and increasing insulin sensitivity in vivo.

Tali et al. found that fatty acid binding protein-4 (FABP-4)-null preadipocytes can enhance PPARγ

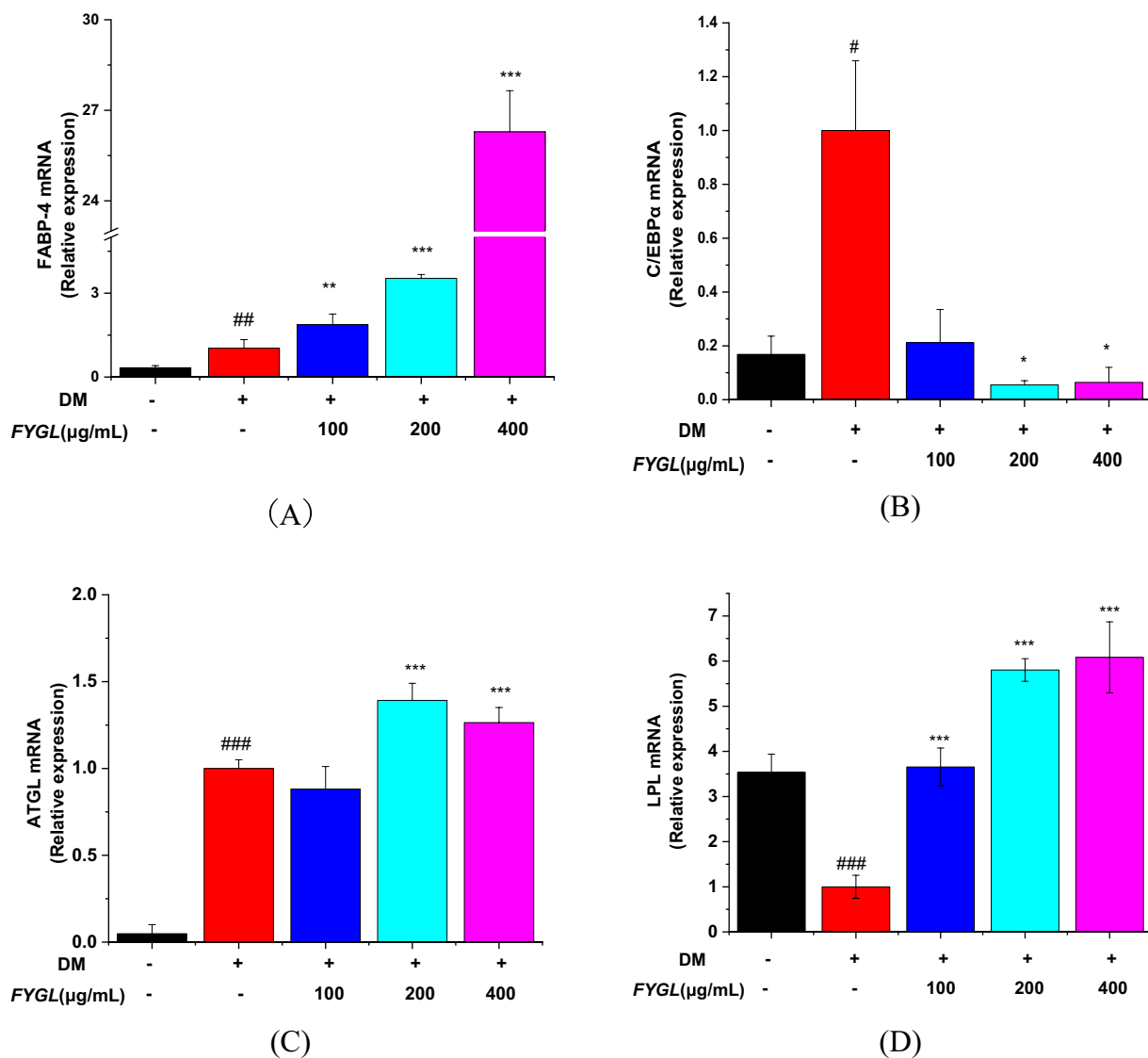


**Fig. 8** The relative mRNA expression levels of (A) C/EBPα, (B) FABP-4, (C) ATGL, and (D) LPL in differentiated 3T3-L1 cells, with reference to the model group. Data are presented as the mean ± S.D. values ( $n=6$ ). ### $P < 0.001$ , ## $P < 0.01$ , # $P < 0.05$  vs. blank control group. \*\*\* $P < 0.001$ , \*\* $P < 0.01$ , \* $P < 0.05$  vs. model group

expression and activity, while the overexpression of FABP-4 inhibits PPAR $\gamma$  expression and adipogenesis [67]. Furuhashi et al. further found that FABP-4-null mice exhibit decreased lipolysis in adipocytes and pancreatic  $\beta$  cells and reduced insulin secretion [68]. The present work proved that *FYGL* could inhibit the differentiation of 3T3-L1 preadipocytes and promote lipolysis in mature adipocytes, therefore reducing lipid droplet accumulation. Studies have shown that fatty acid synthase (FAS) plays an important role in lipogenic pathways, which are involved in fatty acid biosynthesis [57]. In addition, the AMPK $\alpha$  signalling pathway also plays a critical role in lipolysis [19, 58, 60]. ATGL and

HSL catalyse triglyceride degradation, releasing the fatty acids in lipid droplets of adipocytes [69], while adipocytes secrete LPL to degrade triglycerides in very low-density lipoprotein (VLDL) in vessels [70]. The results of present study indicated that *FYGL* promoted the degradation of lipid droplets in mature adipocytes by activating the AMPK $\alpha$  signalling pathway. Taken together, the results of the study on the cellular level showed that *FYGL* could inhibit lipid accumulation by both suppressing the differentiation of preadipocytes and promoting the degradation of lipid droplets in mature adipocytes to alleviate metabolically unhealthy obesity.

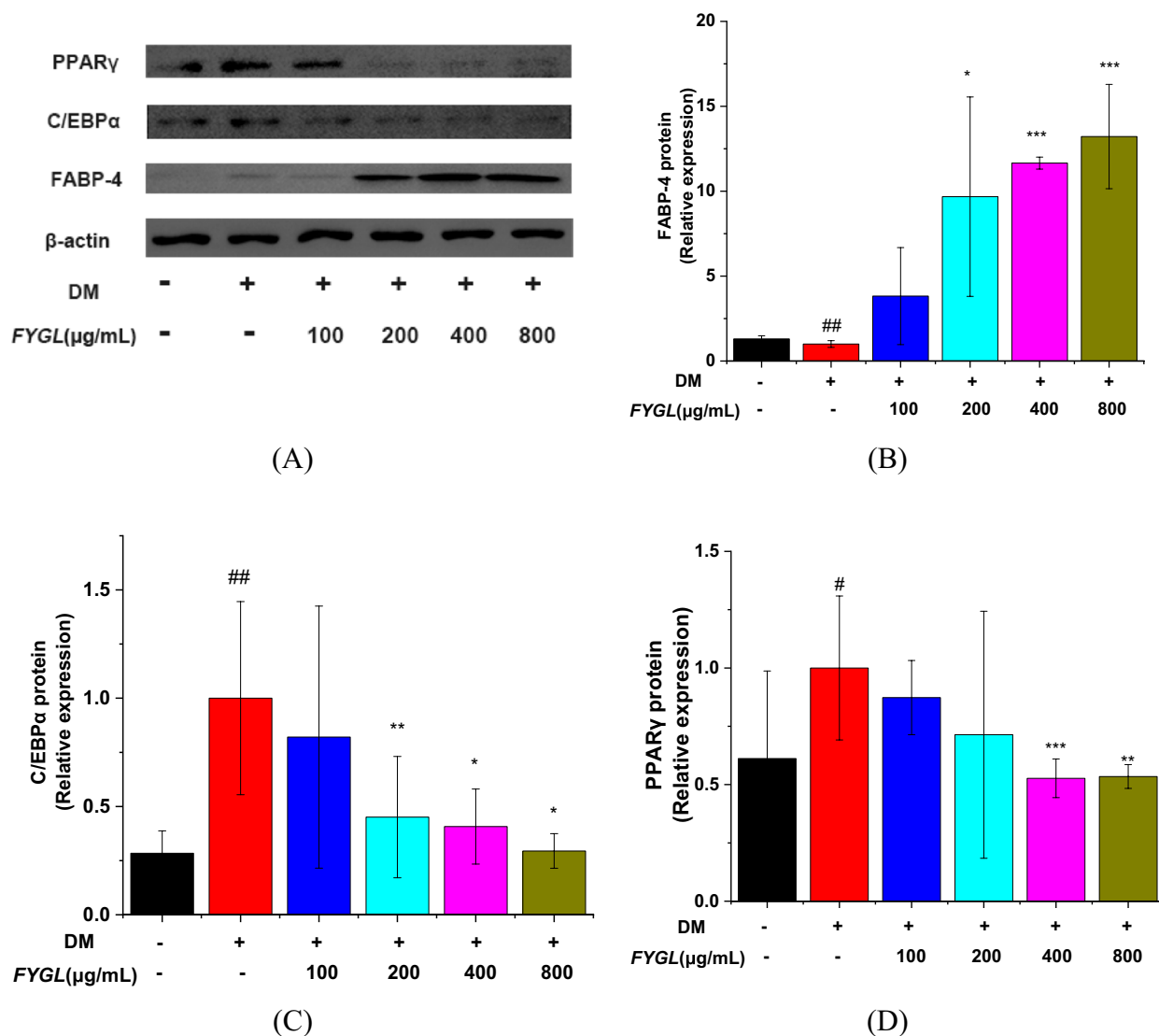


**Fig. 9** Western blot analysis of proteins involved in cellular differentiation in mature 3T3-L1 cells. **A** Images of the PPAR $\gamma$ , C/EBP $\alpha$ , and FABP-4 protein bands relative to the  $\beta$ -actin protein band. **B**, **C** and **D** Relative expression of PPAR $\gamma$ , C/EBP $\alpha$ , and FABP-4, respectively, with reference to  $\beta$ -actin, and normalized to the model group. Data are presented as the mean  $\pm$  S.D. values ( $n=3$ ). ## $P < 0.01$ , # $P < 0.05$  vs. blank control group, \*\*\* $P < 0.001$ , \*\* $P < 0.01$ , \* $P < 0.05$  vs. model group

**Strengths and limitations of FYGL compared with reported work**

In recent years, some natural medicinal plants have been used in the treatment of obesity and metabolic diseases because of their safety [71]. *Hibiscus rosa-sinensis* flowers were reported to be capable of decreasing obesity by reducing adipogenesis and activating AMPK to promote fatty acid oxidation [11]. *Momordica charantia* extracts can activate the AMPK signalling pathway, reduce adipogenic gene expression and peroxisome proliferator-activated receptor (PPAR) signalling in adipose tissue, and increase lipid oxidation in adipose tissue, thereby

reducing obesity and insulin resistance [72, 73]. In addition, cannabidiol can promote adipocyte browning for the treatment of metabolic diseases [74].

Because FYGL is a macromolecular proteoglycan, it has multiple diabetes related-targets, such as protein tyrosine phosphatase 1B (PTP1B, a receptor of insulin resistance [31]),  $\alpha$ -glucosidase [36] and amylin [75] through  $\pi$ - $\pi$  stacking between aromatic groups in proteins as well as hydrogen bonding between protein and saccharide. These properties provide the basis of FYGL efficacy. FYGL also has anti-oxidation because of its reductive sugar residues. Therefore, FYGL play multiple roles by multiple targets

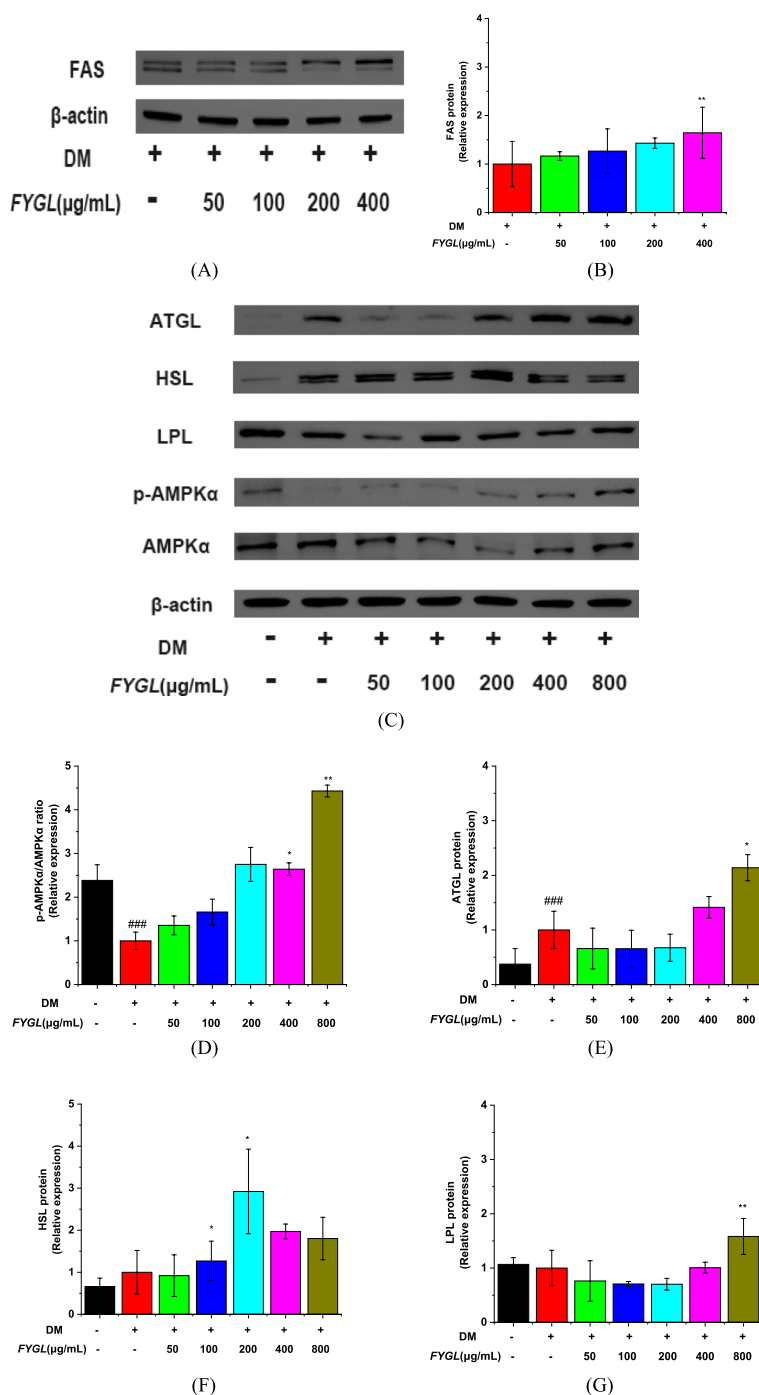


**Fig. 10** Western blot analysis of proteins involved in lipolysis and the AMPKα signalling pathway in mature 3T3-L1 cells. **A** Image of FAS protein bands, **B** Quantification of FAS expression. **C** Images of ATGL, HSL, LPL, p-AMPKα, and AMPKα protein bands. **D, E, F** and **G** Quantification of ATGL, HSL, LPL, and p-AMPKα/AMPKα protein levels, respectively. The protein levels in the model group are normalized to a value of 1.0. Data are presented as the mean ± S.D. values (n = 3). ###p < 0.01, ###p < 0.001 vs. blank control group, \*p < 0.01, \*p < 0.05 vs. model group

on alleviating blood glucose [28], improving the lipid metabolism [54], reducing the diabetes-induced reactive oxygen species [37] and regulating immunity [76], in addition to specific action against obesity-induced

diabetes. Importantly, *FYGL* is highly safe with LD50 of 6 g/kg [31], much safer than clinic anti-obesity drugs, such as orlistat and liraglutide. *FYGL* is an ingredient of macromolecules with a molecular weight distribution,

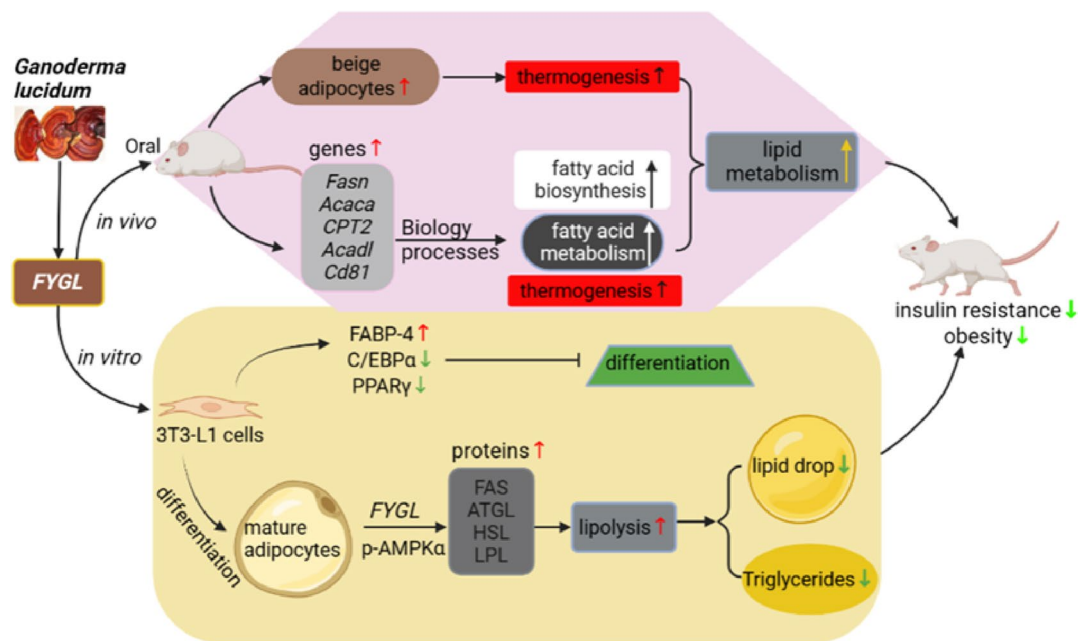


**Fig. 11** Profile of the mechanism of *FYGL* in ameliorating obesity-induced diabetes

which limits one to characterize its molecular structure as clearly as small molecules but could allow it to act multiple functions.

It should be mentioned that *FYGL* is a macromolecular proteoglycan with multi-targets and multi-pathways to regulate obesity-induced diabetes. Its effective dose in clinic could not be converted simply from mice to human on the body weight like the common small molecular drug does. Especially for a targeting drug, different genus may have different responses and sensitivity. In addition, *FYGL* include amino acids and saccharides, consistent to those present in blood and urine, therefore, it is difficult to follow the tracks of *FYGL* when it was orally administered and possibly decomposed in stomach. Previously, we studied the distribution of Cy5-labeled *FYGL* in mice and found that *FYGL* was available in small intestine and viscera, and enriched mostly in liver, and excreted from the body after 12 h [76].

## Conclusion

This study showed that *FYGL* could increase the number of beige adipocytes and restore adipocyte morphology, thereby alleviating metabolic disorders in *db/db* mice. The mechanism *in vivo* by which *FYGL* alleviates metabolic disorders involves the balance between fatty acid biosynthesis and metabolism to effectively dissipate energy in beige adipocytes. *In vitro*, *FYGL* inhibited the differentiation of preadipocytes by increasing FABP-4 gene expression and decreasing PPAR $\gamma$  and C/EBP $\alpha$  gene levels. Moreover, *FYGL* promoted adipocyte

browning by upregulating *Cd81* gene expression. Furthermore, *FYGL* increased the levels of the lipolysis-related proteins of ATGL, HSL and LPL by activating the AMPK $\alpha$  signalling pathway, therefore accelerating lipid metabolism in mature adipocytes. Importantly, these findings proved that *FYGL*, a proteoglycan, could modify metabolic disorders by targeting both preadipocytes and mature adipocytes. The mechanistic profile of *FYGL* in the treatment of obesity-induced diabetes is shown in Fig. 11. Hopefully, *FYGL* could be used as an agent to treat lipid metabolism disorders and obesity in the clinic.

## Supplementary Information

The online version contains supplementary material available at <https://doi.org/10.1186/s12944-023-01880-6>.

- Additional file 1.
- Additional file 2.
- Additional file 3.
- Additional file 4.
- Additional file 5.

## Acknowledgements

Not applicable.

## Authors' contributions

Y.W: design, acquisition, analysis and interpretation of data, writing of the draft and final manuscript version. F.Y: interpretation of data, revision of the draft. X.Z: revision of the draft. J.L: analysis of data. Z.Z: interpretation of data. Q.Z: revision of the draft. J.C: analysis of data. Y.H: interpretation of data, funding support. H.Y: design of the work, funding support. P.Z: design of the work,



funding support, writing, reviewing and editing of the manuscript. All authors read and approved the final manuscript.

### Funding

This research was funded by the National Natural Science Foundation of China (Nos. 21374022 and 81374032); National Health Commission of the People's Republic of China (No. 2017ZX09301006); Science and Technology Commission of Shanghai Municipality (No. 17401902700); Clinical Research Plan of SHDC (No. SHDC12019124); and Shanghai Collaborative Innovation Center of Industrial Transformation of Hospital TCM Preparation.

### Availability of data and materials

The data presented in this study are available within the article.

### Declarations

#### Ethics approval and consent to participate

The study was conducted in accordance with the Declaration of Helsinki and approved by the Ethics Committee of Fudan University (No. FE21038, 5 March 2021).

#### Consent for publication

Not applicable.

#### Competing interests

The authors declare that they have no competing interests.

Received: 7 April 2023 Accepted: 21 July 2023

Published online: 08 August 2023

### References

- Chatterjee S, Khunti K, Davies MJ. Type 2 diabetes. *Lancet*. 2017;389:2239–51.
- Tong Y, Xu S, Huang L, Chen C. Obesity and insulin resistance: Pathophysiology and treatment. *Drug Discovery Today*. 2022;27:822–30.
- Nathan DM. Diabetes advances in diagnosis and treatment. *Jama-J Am Med Assoc*. 2015;314:1052–62.
- Dhurandhar NV. What is obesity? *Int J Obes*. 2022;46:1081–2.
- Czech MP. Mechanisms of insulin resistance related to white, beige, and brown adipocytes. *Molecular Metabolism*. 2020;34:27–42.
- Gustafson B, Hedjazifar S, Gogg S, Hammarstedt A, Smith U. Insulin resistance and impaired adipogenesis. *Trends Endocrinol Metab*. 2015;26:193–200.
- Romao JM, Guan LL. Chapter 21 - Adipogenesis and Obesity. In: Sen CK, editor. *MicroRNA in Regenerative Medicine*. Oxford: Academic Press; 2015. p. 539–65.
- Hansen Jacob B, Kristiansen K. Regulatory circuits controlling white versus brown adipocyte differentiation. *Biochemical Journal*. 2006;398:153–68.
- Yang FT, Stanford KI. Batokines: mediators of inter-tissue communication (a Mini-Review). *Curr Obes Rep*. 2022;11:1–9.
- Wu M, Liu D, Zeng R, Xian T, Lu Y, Zeng G, Sun Z, Huang B, Huang Q. Epigallocatechin-3-gallate inhibits adipogenesis through down-regulation of PPAR $\gamma$  and FAS expression mediated by PI3K-AKT signaling in 3T3-L1 cells. *Eur J Pharmacol*. 2017;795:134–42.
- Linges A, Paul D, Naidu VGM, Satheeshkumar N. AMPK activating and anti adipogenic potential of Hibiscus rosa sinensis flower in 3T3-L1 cells. *J Ethnopharmacol*. 2019;233:123–30.
- Otto TC, Lane MD. Adipose development: from stem cell to adipocyte. *Crit Rev Biochem Mol Biol*. 2005;40:229–42.
- Tang QQ, Lane MD. Adipogenesis: from stem cell to adipocyte. *Annu Rev Biochem*. 2012;81:715–36.
- Cristancho AG, Lazar MA. Forming functional fat: a growing understanding of adipocyte differentiation. *Nat Rev Mol Cell Biol*. 2011;12:722–34.
- Lehrke M, Lazar MA. The many faces of PPAR $\gamma$ . *Cell*. 2005;123:993–9.
- Sun Z, Gong J, Wu L, Li P. Chapter 14 - Imaging Lipid Droplet Fusion and Growth. In: Yang H, editor. *Methods in Cell Biology*, vol. 116. Li P: Academic Press; 2013. p. 253–68.
- Bosch M, Parton RG, Pol A. Lipid droplets, bioenergetic fluxes, and metabolic flexibility. *Semin Cell Dev Biol*. 2020;108:33–46.
- Klemm RW, Ikonen E. The cell biology of lipid droplets: More than just a phase. *Semin Cell Dev Biol*. 2020;108:1–3.
- Herzig S, Shaw RJ. AMPK: guardian of metabolism and mitochondrial homeostasis. *Nat Rev Mol Cell Biol*. 2018;19:121–35.
- López M. EJE PRIZE 2017: Hypothalamic AMPK: a golden target against obesity? *Eur J Endocrinol*. 2017;176:R235–46.
- Aaseth J, Ellefsen S, Alehagen U, SundfØr TM, Alexander J. Diets and drugs for weight loss and health in obesity – An update. *Biomed Pharmacother*. 2021;140:111789.
- Lingvay I, Sumithran P, Cohen RV, Le Roux CW. Obesity management as a primary treatment goal for type 2 diabetes: time to reframe the conversation. *Lancet*. 2022;399:394–405.
- Liu TT, Liu XT, Chen QX, Shi Y. Lipase inhibitors for obesity: a review. *Biomed Pharmacother*. 2020;128:110314.
- Drucker DJ. Mechanisms of Action and Therapeutic Application of Glucagon-like Peptide-1. *Cell Metab*. 2018;27:740–56.
- Foretz M, Guigas B, Viollet B. Understanding the gluco-regulatory mechanisms of metformin in type 2 diabetes mellitus. *Nat Rev Endocrinol*. 2019;15:569–89.
- Subhasree PDBaRS. The Sacred Mushroom “Reishi”-A Review. *American-Eurasian Journal of Botany*. 2008;1(3):107–10, 200.
- Bishop KS, Kao CHJ, Xu Y, Glucina MP, Paterson RRM, Ferguson LR. From 2000years of Ganoderma lucidum to recent developments in nutraceuticals. *Phytochemistry*. 2015;114:56–65.
- Teng BS, Wang CD, Zhang D, Wu JS, Pan D, Pan LF, Yang HJ, Zhou P. Hypoglycemic effect and mechanism of a proteoglycan from ganoderma lucidum on streptozotocin-induced type 2 diabetic rats. *Eur Rev Med Pharmacol Sci*. 2012;16:166–75.
- Pan D, Wang L, Chen C, Hu B, Zhou P. Isolation and characterization of a hyperbranched proteoglycan from Ganoderma Lucidum for anti-diabetes. *Carbohydr Polym*. 2015;117:106–14.
- Yu F, Wang Y, Teng Y, Yang S, He Y, Zhang Z, Yang H, Ding C-F, Zhou P. Interaction and Inhibition of a Ganoderma lucidum Proteoglycan on PTP1B Activity for Anti-diabetes. *ACS Omega*. 2021;6:29804–13.
- Teng B-S, Wang C-D, Yang H-J, Wu J-S, Zhang D, Zheng M, Fan Z-H, Pan D, Zhou P. A protein tyrosine phosphatase 1B activity inhibitor from the fruiting bodies of Ganoderma lucidum (Fr.) Karst and its hypoglycemic potency on Streptozotocin-Induced type 2 diabetic mice. *J Agric Food Chem*. 2011;59:6492–500.
- Yang Z, Wu F, He Y, Zhang Q, Zhang Y, Zhou G, Yang H, Zhou P. A novel PTP1B inhibitor extracted from Ganoderma lucidum ameliorates insulin resistance by regulating IRS1-GLUT4 cascades in the insulin signaling pathway. *Food Funct*. 2018;9:397–406.
- Yang Z, Zhang Z, Zhao J, He Y, Yang H, Zhou P. Modulation of energy metabolism and mitochondrial biogenesis by a novel proteoglycan from Ganoderma lucidum. *RSC Adv*. 2019;9:2591–8.
- Pan D, Zhang D, Wu J, Chen C, Xu Z, Yang H, Zhou P. A novel proteoglycan from Ganoderma lucidum fruiting bodies protects kidney function and ameliorates diabetic nephropathy via its antioxidant activity in C57BL/6 db/db mice. *Food Chem Toxicol*. 2014;63:111–8.
- Vohra MS, Ahmad B, Serpell CJ, Parhar IS, Wong EH. Murine in vitro cellular models to better understand adipogenesis and its potential applications. *Differentiation*. 2020;115:62–84.
- Zhang Y, Pan Y, Li J, Zhang Z, He Y, Yang H, Zhou P. Inhibition on  $\alpha$ -glucosidase activity and non-enzymatic glycation by an anti-oxidative proteoglycan from ganoderma lucidum. *Molecules*. 2022;27:1457.
- Pan Y, Yuan S, Teng Y, Zhang Z, He Y, Zhang Y, Liang H, Wu X, Li J, Yang H, Zhou P. Antioxidation of a proteoglycan from Ganoderma lucidum protects pancreatic  $\beta$ -cells against oxidative stress-induced apoptosis in vitro and in vivo. *Int J Biol Macromol*. 2022;200:470–86.
- Zebisch K, Voigt V, Wabitsch M, Brandsch M. Protocol for effective differentiation of 3T3-L1 cells to adipocytes. *Anal Biochem*. 2012;425:88–90.
- Liang H, Pan Y, Teng Y, Yuan S, Wu X, Yang H, Zhou P. A proteoglycan extract from Ganoderma Lucidum protects pancreatic beta-cells against STZ-induced apoptosis. *Biosci Biotechnol Biochem*. 2020;84:2491–8.
- Kane JP, Pullinger CR, Goldfine ID, Malloy MJ. Dyslipidemia and diabetes mellitus: role of lipoprotein species and interrelated pathways of lipid metabolism in diabetes mellitus. *Curr Opin Pharmacol*. 2021;61:21–7.

41. Ceperuelo-Mallafre V, Ejarque M, Serena C, Duran X, Montori-Grau M, Rodríguez MA, Yanes O, Núñez-Roa C, Roche K, Puthanveetil P, et al. Adipose tissue glycogen accumulation is associated with obesity-linked inflammation in humans. *Molecular Metabolism*. 2016;5:5–18.
42. Wallace M, Metallo CM. Tracing insights into de novo lipogenesis in liver and adipose tissues. *Semin Cell Dev Biol*. 2020;108:65–71.
43. Munday MR. Regulation of mammalian acetyl-CoA carboxylase. *Biochem Soc Trans*. 2002;30:1059–64.
44. Hsiao Y-S, Jogl G, Esser V, Tong L. Crystal structure of rat carnitine palmitoyltransferase II (CPT-II). *Biochem Biophys Res Commun*. 2006;346:974–80.
45. Chen Y, Ren Q, Zhou Z, Deng L, Hu L, Zhang L, Li Z. HWL-088, a new potent free fatty acid receptor 1 (FFAR1) agonist, improves glucolipid metabolism and acts additively with metformin in ob/ob diabetic mice. *Br J Pharmacol*. 2020;177:2286–302.
46. Jaiswal M, Schinske A, Pop-Busui R. Lipids and lipid management in diabetes. *Best Pract Res Clin Endocrinol Metab*. 2014;28:325–38.
47. Taskinen M-R, Borén J. New insights into the pathophysiology of dyslipidemia in type 2 diabetes. *Atherosclerosis*. 2015;239:483–95.
48. Oguri Y, Shinoda K, Kim H, Alba DL, Bolus WR, Wang Q, Brown Z, Pradhan RN, Tajima K, Yoneshiro T, et al. CD81 controls beige fat progenitor cell growth and energy balance via FAK signaling. *Cell*. 2020;182:563–577. e520.
49. Cléménçon B, Babot M, Trézéguet V. The mitochondrial ADP/ATP carrier (SLC25 family): pathological implications of its dysfunction. *Mol Aspects Med*. 2013;34:485–93.
50. Cohen P, Kajimura S. The cellular and functional complexity of thermogenic fat. *Nat Rev Mol Cell Biol*. 2021;22:393–409.
51. Hay N. Akt isoforms and glucose homeostasis – the leptin connection. *Trends Endocrinol Metab*. 2011;22:66–73.
52. Corrêa-Giannella ML, Machado UF. SLC2A4 gene: a promising target for pharmacogenomics of insulin resistance. *Pharmacogenomics*. 2013;14:847–50.
53. Li G, Zhang L. miR-335-5p aggravates type 2 diabetes by inhibiting SLC2A4 expression. *Biochem Biophys Res Commun*. 2021;558:71–8.
54. Pan Y, Zhang Y, Li J, Zhang Z, He Y, Zhao Q, Yang H, Zhou P. A proteoglycan isolated from *Ganoderma lucidum* attenuates diabetic kidney disease by inhibiting oxidative stress-induced renal fibrosis both in vitro and in vivo. *J Ethnopharmacol*. 2023;310:116405.
55. Rosen ED, MacDougald OA. Adipocyte differentiation from the inside out. *Nat Rev Mol Cell Biol*. 2006;7:885–96.
56. Ali AT, Hochfeld WE, Myburgh R, Pepper MS. Adipocyte and adipogenesis. *Eur J Cell Biol*. 2013;92:229–36.
57. Berndt J, Kovacs P, Ruschke K, Klötting N, Fasshauer M, Schön MR, Körner A, Stumvoll M, Blüher M. Fatty acid synthase gene expression in human adipose tissue: association with obesity and type 2 diabetes. *Diabetologia*. 2007;50:1472–80.
58. Grabner GF, Xie H, Schweiger M, Zechner R. Lipolysis: cellular mechanisms for lipid mobilization from fat stores. *Nat Metab*. 2021;3:1445–65.
59. Walther TC, Farese RV. Lipid droplets and cellular lipid metabolism. *Annu Rev Biochem*. 2012;81:687–714.
60. Wang Y, Rodrigues B. Intrinsic and extrinsic regulation of cardiac lipoprotein lipase following diabetes. *Biochimica et Biophysica Acta (BBA) - Molecular and Cell Biology of Lipids*. 2015;1851:163–71.
61. Cypess AM, Lehman S, Williams G, Tal I, Rodman D, Goldfine AB, Kuo FC, Palmer EL, Tseng Y-H, Doria A, et al. Identification and importance of brown adipose tissue in adult humans. *N Engl J Med*. 2009;360:1509–17.
62. Stock MJ, Cinti S. ADIPOSE TISSUE | Structure and Function of Brown Adipose Tissue. In: Caballero B, editor. *Encyclopedia of Food Sciences and Nutrition (Second Edition)*. Oxford: Academic Press; 2003. p. 29–34.
63. Virtanen KA. Adipose Tissue: Structure and Function of Brown Adipose Tissue. In: Caballero B, Finglas PM, Toldrá F, editors. *Encyclopedia of Food and Health*. Oxford: Academic Press; 2016. p. 30–4.
64. Lidell ME, Betz MJ, Leinhard OD, Heglund M, Elander L, Slawik M, Mussack T, Nilsson D, Romu T, Nuutila P, et al. Evidence for two types of brown adipose tissue in humans. *Nat Med*. 2013;19:631–4.
65. Ouellet V, Routhier-Labadie A, Bellemare W, Lakhali-Chaieb L, Turcotte E, Carpentier AC, Richard D. Outdoor temperature, age, sex, body mass index, and diabetic status determine the prevalence, mass, and glucose-uptake activity of 18F-FDG-detected BAT in humans. *J Clin Endocrinol Metab*. 2011;96:192–9.
66. Kajimura S. Bruce, seal: brown and beige fat: physiological roles beyond heat generation. *Cell Metab*. 2015;22:546–59.
67. Garin-Shkolnik T, Rudich A, Hotamisligil GS, Rubinstein M. FABP4 attenuates PPAR $\gamma$  and adipogenesis and is inversely correlated with PPAR $\gamma$  in adipose tissues. *Diabetes*. 2014;63:900–11.
68. Furuhashi M. Fatty acid-binding protein 4 in cardiovascular and metabolic diseases. *J Atheroscler Thromb*. 2019;26:216–32.
69. Ahmadian M, Abbott Marcia J, Tang T, Hudak Carolyn SS, Kim Y, Bruss M, Hellerstein Marc K, Lee H-Y, Samuel Varman T, Shulman Gerald I, et al. Desnutrin/ATGL is regulated by AMPK and is required for a brown adipose phenotype. *Cell Metab*. 2011;13:739–48.
70. Borén J, Taskinen M-R, Björnson E, Packard CJ. Metabolism of triglyceride-rich lipoproteins in health and dyslipidaemia. *Nat Rev Cardiol*. 2022;19:577–92.
71. Ali Esmail A-S, Muayad Hussein A, Kareema Helal S. Medicinal plants for the treatment of obesity and overweight: A review. *World J Biol Pharm Health Sci*. 2022;10:001–10.
72. Huang HL, Hong YW, Wong YH, Chen YN, Chyuan JH, Huang CJ, Chao PM. Bitter melon (*Momordica charantia* L.) inhibits adipocyte hypertrophy and down regulates lipogenic gene expression in adipose tissue of diet-induced obese rats. *Br J Nutr*. 2008;99:230–9.
73. Ramachandra Shobha C, Prashant V, Akila P, Chandini R, Nataraj Suma M, Basavanagowdappa H. Fifty percent ethanolic extract of *Momordica charantia* inhibits adipogenesis and promotes adipolysis in 3T3-L1 pre-adipocyte cells. *Rep Biochem Mol Biol*. 2017;6:22–32.
74. Parray HA, Yun JW. Cannabidiol promotes browning in 3T3-L1 adipocytes. *Mol Cell Biochem*. 2016;416:131–9.
75. Yu F, Teng Y, Yang S, He Y, Zhang Z, Yang H, Ding C-F, Zhou P. The thermodynamic and kinetic mechanisms of a *Ganoderma lucidum* proteoglycan inhibiting hIAPP amyloidosis. *Biophys Chem*. 2022;280:106702.
76. Teng Y, Liang H, Zhang Z, He Y, Pan Y, Yuan S, Wu X, Zhao Q, Yang H, Zhou P. Biodistribution and immunomodulatory activities of a proteoglycan isolated from *Ganoderma lucidum*. *J Func Foods*. 2020;74:104193.

## Publisher's Note

Springer Nature remains neutral with regard to jurisdictional claims in published maps and institutional affiliations.

Ready to submit your research? Choose BMC and benefit from:

- fast, convenient online submission
- thorough peer review by experienced researchers in your field
- rapid publication on acceptance
- support for research data, including large and complex data types
- gold Open Access which fosters wider collaboration and increased citations
- maximum visibility for your research: over 100M website views per year

At BMC, research is always in progress.

Learn more [biomedcentral.com/submissions](https://biomedcentral.com/submissions)

